Optical Design and Choice of Modulation Frequencies for a LIGO-like LSC Scheme

Kevin Kuns

Technical Note CE–T2400022–v2 October 14, 2024

https://cosmicexplorer.org/

1 Introduction

The length sensing and control (LSC) system used by LIGO to control the five length degrees of freedom is a PDH scheme with two RF modulation frequencies [1]. Cosmic Explorer does not need to use this LSC scheme, but it is a useful baseline concept at this time. This note details some considerations for choosing the modulation frequencies and macroscopic[1] lengths necessary to use such a scheme and gives an example design satisfying these requirements starting with the "Crab" telescope design [2] as it is at the time of this writing.

Section 2 describes the LIGO PDH sensing scheme and derives the required relationships between the RF modulation frequencies and macroscopic cavity lengths needed for it to work. A summary of these requirements is given in Section 2.4 where the example LSC design is derived and summarized in Table 1. The design for LIGO laid out in Ref. [1] started with the modulation frequencies chosen; however, starting from scratch, CE is not so constrained. The approach taken here is therefore to start with the cavity lengths chosen to give the telescopes of interest rather than to start with the modulation frequencies. Section 3 lists some other requirements not considered here which will need to be analyzed before settling on a final design.

2 Sensing Scheme

The LIGO LSC scheme uses two RF sidebands (denoted f_1 and f_2) with different resonance conditions in the various optical cavities of the dual recycled Fabry-Perot Michelson interferometer (DRFPMI). In particular

(1) In the arm cavities, the carrier is resonant and the sidebands are nearly anti-resonant.

(2) In the power recycling cavity (PRC), the carrier and both sidebands are resonant.

(3) In the signal extraction cavity (SEC), the carrier is anti-resonant, the f_2 sidebands are resonant, and the f_1 sidebands are nearly anti-resonant.

These resonance conditions require precise relationships between the cavity lengths and modulation frequencies which are derived in Sections 2.1 and 2.2. Once the macroscopic PRC and SEC lengths are chosen to satisfy these resonance conditions, a macroscopic asymmetry, the Schnupp asymmetry, between the distances between the beamsplitter and the two arm cavities is introduced so that some sideband power leaks from the PRC into the SEC.[2] The Schnupp asymmetry is chosen to maximize the f_2 sideband power resonating in the SEC as is described in Section 2.3.

[1] "Macroscopic" is taken to mean larger than the 1 μm laser wavelength in this note.

[2] The macroscopic Schnupp asymmetry is distinct from the microscopic difference in arm lengths introduced between the two arms, the DARM offset, used to leak carrier light into the SEC to use as the local oscillator for DC readout; the Schnupp asymmetry leaks RF sideband, rather than carrier, into the SEC. Nevertheless, this imbalance does introduce noise couplings [3–5].

In the following, L_p and L_s are the distances between the PRM and the beamsplitter and between the SEM and the beamsplitter, respectively; l_x and l_y are the distances between the beamsplitter and ITMX and between the beamsplitter and ITMY, respectively. The length of the PRC and SEC are defined as

$$L_\mathrm{prc} = L_\mathrm{p} + l_+, \qquad L_\mathrm{sec} = L_\mathrm{s} + l_+, \tag{1}$$

where l_+ is the average distance between the beamsplitter and the ITMs. The Schnupp asymmetry l_sch is the difference in the distances between the ITMs and the beamsplitter in both arms:

$$l_\pm = \frac{l_\mathrm{x} \pm l_\mathrm{y}}{2}, \qquad l_\mathrm{sch} = 2l_-. \tag{2}$$

Note that these are optical, rather than physical, path lengths in this note and therefore account for the ITM and beamsplitter substrates.

Since the language is confusing, the precise definition of a field being "resonant" or "anti-resonant" should be used: if F is the open loop gain of a field in an optical cavity, that cavity is said to be

- resonant if $\arg F = 2\pi n$, i.e. the round-trip phase is 0°
- anti-resonant if $\arg F = (2n+1)\pi$, i.e. the round-trip phase is 180°

for any integer n.

2.1 Arm cavities

The reflection of a field of frequency ω off of the arm cavities is

$$r_\mathrm{a}(\omega) = \frac{r_\mathrm{i} - (1-\mathcal{L}_\mathrm{i}) r_\mathrm{e} \mathrm{e}^{-2\mathrm{i}\omega L_\mathrm{a}/c}}{1 - r_\mathrm{i} r_\mathrm{e} \mathrm{e}^{-2\mathrm{i}\omega L_\mathrm{a}/c}} \tag{3}$$

where L_a is the arm cavity length, $r_\mathrm{i,e}$ are the amplitude reflectivities of the ITM and ETM, respectively, $\mathcal{L}_\mathrm{i}$ is the power loss of the ITM, and c is the speed of light. In an interferometer the arm cavities are strongly overcoupled with $r_\mathrm{e} \approx 1$ and have low loss with $\mathcal{L}_\mathrm{i} \ll 1$. Thus, to a good approximation,

$$r_\mathrm{a}(\omega_0) = -1 \tag{4a}$$

$$r_\mathrm{a}\left(\omega_0 + \Omega_i\right) = \mathrm{e}^{\mathrm{i}\theta_i} \approx 1, \tag{4b}$$

where θ_i is the phase that the ith RF sidebands of frequency Ω_i pick up on reflection from the arm cavity. If the sidebands were exactly anti-resonant $2(\omega_0+\Omega_i)L_\mathrm{a}/c = \pi$ and so $\theta_i = 0$. In reality they will in general acquire a small phase shift. The example of Section 2.4, with $m = 76$ and $N = 7$, for instance, have $\theta_1 = 0.43°$ and $\theta_2 = -0.25°$. It is possible for the sidebands to pick up a large phase shift if they happen to be closer to resonance—the $m = 67$ and $N = 7$ case with $f_1 \approx 11\,\mathrm{MHz}$ and $f_2 \approx 80\,\mathrm{MHz}$ have $\theta_1 \approx 136°$ and $\theta_2 \approx 39°$ to take an extreme example—however, this should be checked and these choices of frequencies avoided. Therefore, θ_i can be taken to be zero in the following analysis.

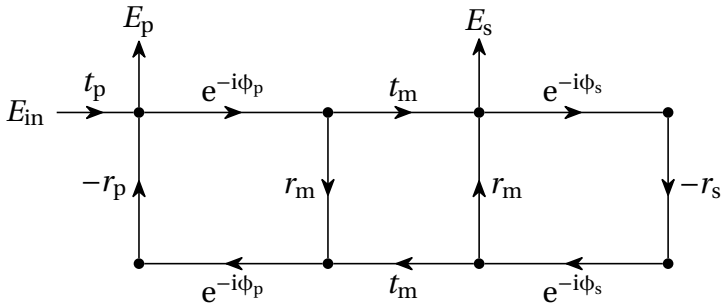

Figure 1: Signal flow diagram of the fields in the corner of a DRFPMI where E_{in} is the field entering the interferometer incident on the back of the PRM, E_p is the field in the PRC, and E_s is the field in the SEC. The left most loop is the PRC and the right most loop is the SEC. The one-way phases ϕ_p and ϕ_s correspond to the phase accumulated by a field propagating over the distances defined in Eq. (1), and the Michelson reflection r_m and transmission t_m are given by Eq. (5). The gain for the sidebands in the SEC, $G_{sec} = |E_s/E_{in}|^2$, can be calculated by performing Gaussian elimination as described in Appendix A and illustrated for the f_2 sidebands in Fig. 4.

2.2 Power recycling and signal extraction cavities

The signal flow diagram for the fields in the corner of a DRFPMI is shown in Fig. 1. The reflection and transmission of the Michelson degree of freedom formed by the beamsplitter and arm cavities are

$$r_m(\omega) = r_a(\omega)\, e^{-2i\omega l_+/c} \cos\left(\frac{\omega l_{sch}}{c}\right) \tag{5a}$$

$$t_m(\omega) = -i r_a(\omega)\, e^{-2i\omega l_+/c} \sin\left(\frac{\omega l_{sch}}{c}\right). \tag{5b}$$

From Fig. 1, the open loop gain of the PRC is

$$F_p(\omega) = -r_p r_m(\omega) e^{-2i\omega L_p/c} = -r_p r_a(\omega) e^{-2i\omega L_{prc}/c} \cos\left(\frac{\omega l_{sch}}{c}\right). \tag{6}$$

Since $\omega l_{sch}/c \ll 1$, having the carrier be resonant in the PRC requires

$$\arg F_p(\omega_0) = \pi + \pi - \frac{2\omega_0 L_{prc}}{c} = 2\pi n. \tag{7}$$

Thus, in order for the sidebands to be resonant,[3]

$$\arg F_p\left(\omega_0 + \Omega_i\right) = \pi + 0 + 0 - \frac{2\Omega_i L_{prc}}{c} = 2\pi n, \tag{8}$$

which requires

$$\Omega_i = \frac{c\pi}{2L_{prc}}(2n+1), \qquad i = 1, 2. \tag{9}$$

[3]We are here sloppy and use n, m, k, etc. to denote arbitrary integers and aren't careful about redefinitions such as $n \to n - 1$.

Similarly, the open loop gain of the SEC is

$$F_{\rm s}(\omega) = -r_{\rm s} r_{\rm m}(\omega) {\rm e}^{-2{\rm i}\omega L_{\rm s}/c} = -r_{\rm s} r_{\rm a}(\omega) {\rm e}^{-2{\rm i}\omega L_{\rm sec}/c} \cos\left(\frac{\omega l_{\rm sch}}{c}\right). \tag{10}$$

Since we use resonant sideband extraction (RSE), the carrier must be *anti-resonant*[4] in the SEC which requires

$$\arg F_{\rm s}(\omega_0) = \pi + \pi - \frac{2\omega_0 L_{\rm sec}}{c} = 2\pi(n+1). \tag{11}$$

Thus, in order for the f_2 sidebands to be resonant in the SEC

$$\arg F_{\rm s}\left(\omega_0 + \Omega_2\right) = \pi + 0 + \pi - \frac{2\Omega_2 L_{\rm sec}}{c} = 2\pi m \tag{12}$$

which requires

$$\Omega_2 = \frac{c\pi}{L_{\rm sec}} m, \qquad \Omega_1 \neq \frac{c\pi}{L_{\rm sec}} k \tag{13}$$

for the f_1 sidebands to also be non-resonant in the SEC.

2.3 Schnupp asymmetry

Once the sideband frequencies and macroscopic cavity lengths are chosen, the Schnupp asymmetry must be introduced so that some sideband power can leak into and resonate in the SEC. The gain of the f_2 sideband in the SEC Eq. (27) is derived in Appendix A where it is shown that, in the high finesse limit, the optimal Schnupp asymmetry which maximizes the power of the f_2 sidebands in the SEC is

$$l_{\rm sch} = \frac{c}{2 f_2 \sqrt{\mathcal{F}_{\rm p}\mathcal{F}_{\rm s}}} \tag{14}$$

where the PRC and SEC cavity finesses are

$$\mathcal{F}_{\rm p,s} = \frac{\pi}{1 - r_{\rm p,s}}. \tag{15}$$

This optimal asymmetry results in a gain for the f_2 sidebands of

$$G_{\rm sec} = \frac{P_{\rm s}}{P_{\rm in}} = \frac{\mathcal{F}_{\rm s}}{2\pi}, \tag{16}$$

[4]This terrible terminology is due to the fact that with the arms off resonance, i.e. in a dual recycled Michelson interferometer ($r_{\rm e} = 0$), the carrier should be "resonant" in the SEC to recover the signal extraction condition because the carrier does not pick up the extra π phase shift on reflection of a resonant cavity. As always, one should think about phases, and signal extraction requires the carrier to have a round-trip π phase shift so that the open loop gain of the SEC is positive and the audio signal sidebands are enhanced above the arm cavity pole when the round-trip phase again flips sign.

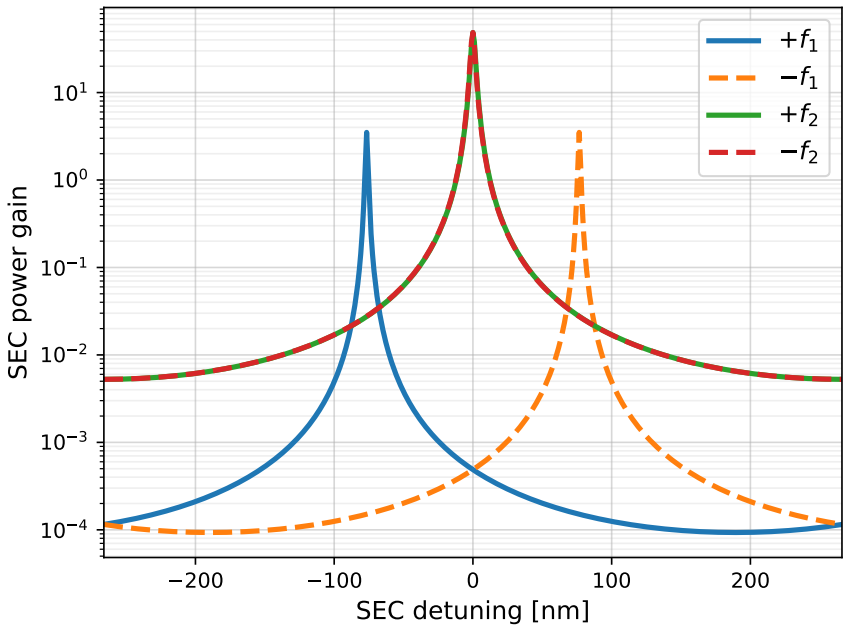

Figure 2: Ratio of the power in the SEC to the input power for each sideband, G_{sec}, as the SEC length is scanned for the parameters in Table 1.

where P_s is the f_2 sideband power in the SEC and P_{in} is the f_2 sideband power entering the interferometer incident on the back of the PRM. The choice Eq. (14) corresponds to a Michelson transmission for the f_2 sideband into the SEC of

$$T_m = |t_m|^2 = \frac{\pi^2}{\mathcal{F}_p \mathcal{F}_s} = \frac{T_p T_s}{4}. \tag{17}$$

Notably, this is significantly less than T_s which would correspond to "critically coupling" the f_2 sideband into the SEC. The goal is to maximize the f_2 power resonating in the SEC rather than maximizing the f_2 power transmitted through the AS port.

The optimal length given by Eq. (14) is a good approximation for high finesse cavities and when the reflection phase from the arms θ_2 is very small. However, phases of a few degrees and/or higher order finesse corrections can shift this slightly and an exact calculation should be made when choosing the precise length. Figure 3 shows the exact SEC gain as a function of Schnupp asymmetry for the parameters of Table 1

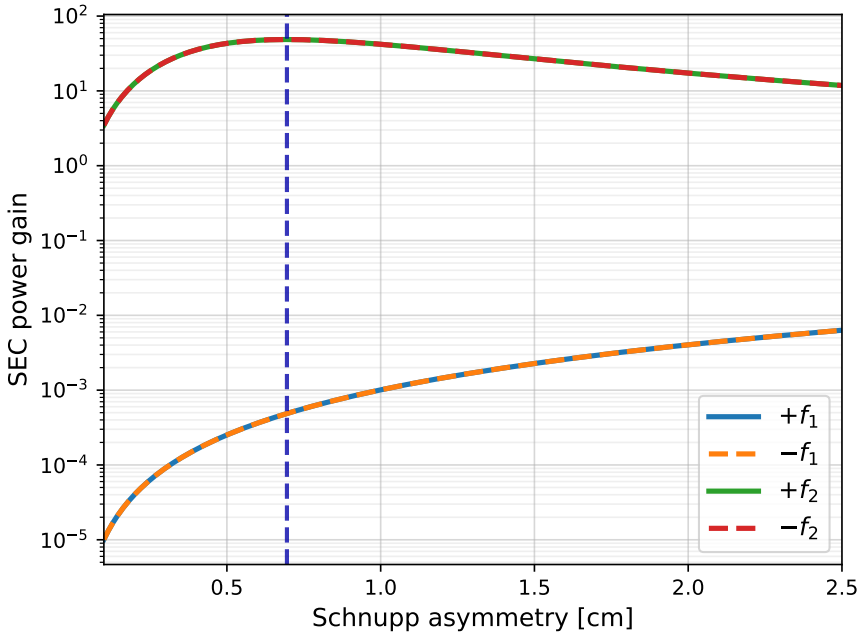

Figure 3: Ratio of the power in the SEC to the input power for each sideband, G_{sec}, as a function of Schnupp asymmetry for the parameters in Table 1.

2.4 Summary and example

The resonance requirements Eqs. (9) and (13) on the RF sideband frequencies for a LIGO-like LSC scheme can be summarized as

$$f_1 = \frac{\Omega_1}{2\pi} = \frac{c}{4L_{\text{prc}}}(2n+1) \neq \frac{c}{2L_{\text{sec}}}k \tag{18a}$$

$$f_2 = \frac{\Omega_2}{2\pi} = (2q+1)f_1 \equiv Nf_1 = \frac{c}{2L_{\text{sec}}}m. \tag{18b}$$

If Eq. (9) is satisfied for f_1, it is automatically satisfied for f_2 if f_2 is an odd integer multiple of f_1. Equation (18) can be translated into equivalent requirements on the macroscopic cavity lengths as

$$L_{\text{prc}} = \frac{c}{4f_1}(2n+1) \tag{19a}$$

$$L_{\text{sec}} = \frac{cm}{2f_2} \neq \frac{ck}{2f_1}. \tag{19b}$$

The design of the LSC scheme used by LIGO described in Ref. [1] started with the sideband frequencies fixed. These were chosen with $f_2 = 5f_1$ to resonate in the input mode cleaner (IMC), however there is no requirement that $N = 5$ for this scheme to work. The LIGO design thus started by choosing macroscopic cavity lengths to satisfy Eq. (19).

Cosmic Explorer is less constrained at this time and can choose cavity lengths and frequencies together. The design of the telescopes is of critical importance to the sensitivity of the detector, in particular determining the the high frequency sensitivity and influencing the difficulty of minimizing squeezing degradations and maximizing power recycling gains. A reasonable strategy is thus to start by designing the telescopes and then to follow the following steps.

(1) The difficulty in building the RF electronics needed to generate the sidebands dictates that the sidebands be between about 10 and 100 MHz, so at no time should f_1 or f_2 be chosen outside of this range.

(2) Since the SEC length directly determines the detector sensitivity and since the most important cavity to mode match to the arms in order to reduce squeezing degradations is the SEC [6], start with $L_{\rm sec}$ fixed by the telescope design and choose f_2 to satisfy Eq. (18b) subject to Item (1), i.e. choose m.

(3) Set f_1 by choosing an N such that m/N is not an integer. Satisfying Item (1) means that N can be 3, 5, 7, or 9.

(4) With f_1 set, choose $L_{\rm prc}$ such that Eq. (19a) is satisfied with the PRC telescope design in mind, i.e. choose n so that $L_{\rm prc}$ is close to that of the desired telescope.

(5) Choose the Schnupp asymmetry $l_{\rm sch}$ to maximize the f_2 power in the SEC. The optimal Schnupp asymmetry is given by Eq. (14) to a good approximation for interferometers such as CE with high finesse cavities. Note that this does not correspond to "critically coupling" the f_2 sideband into the SEC. This optimal $l_{\rm sch}$ is shorter for higher f_2.

(6) Consider other aspects of the detector design not directly related to the corner design, some of which are described in Section 3, and iterate as necessary.

One example of modulation frequencies and cavity lengths chosen to satisfy Eqs. (18) and (19) following the above strategy is shown in Table 1 starting with the "Crab" telescope design [2] as it is at the time of this writing. Figure 2 shows a microscopic scan of the SEC length illustrating the resonance conditions of the f_1 and f_2 sidebands in that cavity, and Fig. 3 shows the SEC gain for both sidebands as a function of Schnupp asymmetry. This exact calculation, rather than the approximation Eq. (14), should be used in general when choosing precise parameters.

3 Other considerations

The following have not been considered but will also impact the exact details of an LSC scheme.

(1) Both sidebands will need to resonate in the input mode cleaners (IMCs) and the IMC lengths will need to be chosen accordingly. Some details about the choice of IMC

Parameter	Symbol	Units	Value
SEC Length	$L_{\rm sec}$	m	125.359
PRC Length	$L_{\rm prc}$	m	248.251
Arm Length	$L_{\rm a}$	km	40.0
ITM transmission	$T_{\rm i}$	%	1.4
SEM transmission	$T_{\rm s}$	%	2.0
PRM transmission	$T_{\rm p}$	%	3.0
f_1 modulation frequency	f_1	MHz	12.982
f_2 modulation frequency	f_2	MHz	90.873
Schnupp asymmetry	$l_{\rm sch}$	cm	0.7
Avg. BS-ITM distance	l_+	m	95.218
f_1 arm reflection phase	θ_1	deg	0.43
f_2 arm reflection phase	θ_2	deg	−0.25
f_2 Michelson transmission	$T_{\rm m}$	%	0.02
f_2 SEC gain	$G_{\rm sec}$	—	50

Table 1: Example parameters satisfying the resonance conditions Eqs. (18) and (19) with $m = 76$ and $N = 7$ starting from the "Crab" telescope design at the time of this writing. The modulation frequencies are rounded to the nearest kHz. A scan of the Schnupp asymmetry is shown Fig. 3; the values of $l_{\rm sch}$, $G_{\rm sec}$, and $T_{\rm m}$ are the optimal values that maximize $G_{\rm sec}$. Distances are optical lengths.

lengths are given in Ref. [7] and this will have a large impact on the laser stabilization and input optics design.

(2) The output mode cleaners (OMCs) need to sufficiently filter all RF sidebands. The choice of RF sideband frequencies will thus influence the OMC design and squeezing losses in the readout.

(3) The lower order higher order modes (HOMs) of the RF sidebands should not be resonant in the arm cavities. The precise arm cavity geometry, which will be chosen in part to ensure that the carrier HOM resonances are not in particularly bad locations for squeezing degradations, will be a major factor determining this. Other considerations, such as PI gains, will also need to be analyzed.

(4) The RF sideband HOMs should also not resonate in the PRC and SEC. LIGO currently suffers from the power recycling gain of the 9 MHz sidebands dropping, and the subsequent loss of error signals derived from these sidebands, as the interferometer thermalizes. This is due to 9 MHz HOMs becoming resonant in the PRC as the Gouy phase of the cavity changes during thermalization. While it is hoped that the introduction of the CHETA subsystem [8] will keep the interferometer in a constant thermal state, the CE LSC design should nevertheless ensure that it has a robust, even if different, sensing scheme for all thermal states, and this will depend on the Gouy phases of the cavities.

(5) No analysis of the angular sensing and control (ASC) scheme as been made. LIGO

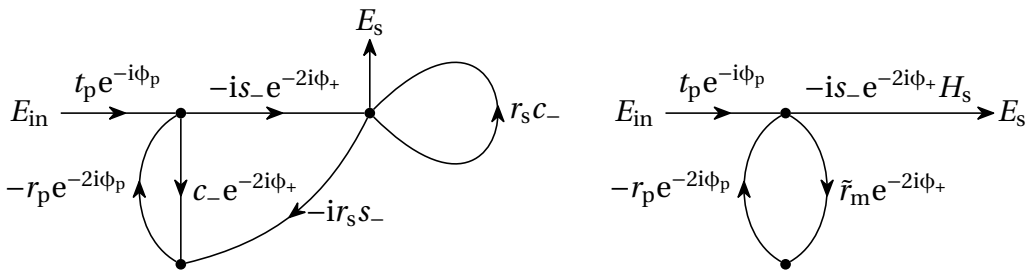

Figure 4: Gaussian elimination of the signal flow diagram Fig. 1 for the f_2 sidebands. The closed loop SEC propagator H_s is given by Eq. (21), the coefficient $\tilde{r}_m$ is given by Eq. (23), $c_- = \cos 2\phi_-$, and $s_- = \sin 2\phi_-$.

uses the same RF sidebands discussed here ($f_1 = 9\,\text{MHz}$ and $f_2 = 5f_1 = 45\,\text{MHz}$) used for the LSC error signals to derive the ASC error signals and has added additional sidebands at $13f_1 = 118\,\text{MHz}$. An analysis of the ASC sensing matrix will need to be made, which will depend heavily on the SEC and PRC Gouy phases, to evaluate the choice of sideband frequencies and the necessity of adding any additional sidebands. The SEC and PRC Gouy phases will, in turn, be chosen in large part to reduce squeezing degradations and increase power recycling gain.

(6) The process of lock acquisition should be considered since different error signals will be used during this period. It is also necessary to reach the desired thermal state which may require different error signals.

A Schnupp asymmetry and SEC gain details

In this appendix we derive the power of the f_2 sideband in the SEC and compute the optimal Schnupp asymmetry that maximizes this power. The left diagram in Fig. 4 shows the partially reduced signal flow diagram of Fig. 1 for the special case of the f_2 sidebands where the Eq. (18) resonance conditions have been used to simplify the propagators. This can be done easily by noting that the round-trip propagation of the carrier in the SEC is π and that ϕ_{sec} for the f_2 sideband must then be chosen to have the open-loop gain of the SEC be positive. Similarly, ϕ_{prc} is chosen to have the open-loop gain of the PRC for the f_2 sideband be positive when the round-trip phase of the carrier is 0. The Michelson transmission and reflection Eq. (5) for the sidebands are

$$r_m(\omega_0 + \Omega_2) = e^{-2i\phi_+} \cos 2\phi_- \approx \left(1 - 2\phi_-^2\right) e^{-2i\phi_+} \tag{20a}$$

$$t_m(\omega_0 + \Omega_2) = -ie^{-2i\phi_+} \sin 2\phi_- \approx -2i\phi_- e^{-2i\phi_-} \tag{20b}$$

The right diagram of Fig. 4 shows the signal flow diagram after eliminating the SEC loop

where the closed loop gain of the SEC is

$$H_\mathrm{s} = \frac{1}{1 - r_\mathrm{s} c_-} = \frac{1}{1 - r_\mathrm{s}} \frac{1}{1 + g_\mathrm{s} \phi_-^2} \tag{21}$$

where

$$g_\mathrm{s,p} = \frac{2 r_\mathrm{s,p}}{1 - r_\mathrm{s,p}}. \tag{22}$$

Note that $g_\mathrm{s,p}\phi_-^2$ is not in general small since $g_\mathrm{s,p} \gg 1$. The reflection term $\tilde{r}_\mathrm{m}$ shown in Fig. 4 is

$$\tilde{r}_\mathrm{m} = c_- - r_\mathrm{s} s_-^2 H_\mathrm{s} = 1 - 2\phi_-^2 \frac{1 + g_\mathrm{s}}{1 + g_\mathrm{s}\phi_-^2} \tag{23}$$

and the closed loop gain of the PRC is, using the f_2 resonance conditions,

$$H_\mathrm{p} = \frac{1}{1 - r_\mathrm{p} \tilde{r}_\mathrm{m}} = \frac{1}{1 - r_\mathrm{p}} \frac{1}{1 + g_\mathrm{p}\phi_-^2 \frac{1+g_\mathrm{s}}{1+g_\mathrm{s}\phi_-^2}}. \tag{24}$$

The transmission of a field incident on the back of the PRM into the SEC, with the f_2 sideband resonance conditions, is therefore

$$\frac{E_\mathrm{s}}{E_\mathrm{in}} = -\mathrm{i} t_\mathrm{p} s_- \mathrm{e}^{-\mathrm{i}(\phi_\mathrm{prc}+\phi_+)} H_\mathrm{p} H_\mathrm{s} = -\mathrm{i}\mathrm{e}^{-\mathrm{i}(\phi_\mathrm{prc}+\phi_+)} \frac{t_\mathrm{p}}{1 - r_\mathrm{p}} \frac{1}{1 - r_\mathrm{s}} \frac{2\phi_-^2}{1 + \phi_-^2(g_\mathrm{s} + g_\mathrm{p} + g_\mathrm{s} g_\mathrm{p})}. \tag{25}$$

In the high finesse limit using the definition of finesse Eq. (15)

$$g_\mathrm{s,p} = \frac{2\mathcal{F}_\mathrm{s,p}}{\pi}\left(1 - \frac{\pi}{\mathcal{F}_\mathrm{s,p}}\right) \approx \frac{2\mathcal{F}_\mathrm{s,p}}{\pi}, \qquad t_\mathrm{s,p}^2 = (1 - r_\mathrm{s,p})(1 + r_\mathrm{s,p}) \approx \frac{4 r_\mathrm{s,p}}{g_\mathrm{s,p}} \tag{26}$$

and the SEC gain is thus

$$G_\mathrm{sec} = \left|\frac{E_\mathrm{s}}{E_\mathrm{in}}\right|^2 \approx \frac{g_\mathrm{p} g_\mathrm{s}^2}{r_\mathrm{s}} \frac{\phi_-^2}{(1 + g_\mathrm{p} g_\mathrm{s} \phi_-^2)^2} = \left(\frac{2\mathcal{F}_\mathrm{p}}{\pi}\right)\left(\frac{2\mathcal{F}_\mathrm{s}}{\pi}\right)^2 \frac{\phi_-^2}{\left(1 + \frac{2\mathcal{F}_\mathrm{p}}{\pi}\frac{2\mathcal{F}_\mathrm{s}}{\pi}\phi_-^2\right)^2}. \tag{27}$$

The ϕ_- that maximizes G_sec is therefore

$$\phi_- = \frac{\Omega_2 l_\mathrm{sch}/2}{c} = \frac{1}{\sqrt{g_\mathrm{p} g_\mathrm{s}}}, \tag{28}$$

which leads to Eq. (14). Plugging this into Eq. (27) gives the maximum SEC gain of Eq. (16), and the Michelson transmission at this optimal length is

$$T_\mathrm{m} = |t_\mathrm{m}|^2 = \sin^2 2\phi_- \approx \frac{4}{g_\mathrm{p} g_\mathrm{s}}, \tag{29}$$

which leads to Eq. (17).

References

[1] G. Mueller, R. Abbott, L. Barsotti, M. Evans, S. Ballmer, V. Frolov, P. Fritschel, and R. Adhikari, "Advanced LIGO length sensing and control final design", LIGO-T1000298 (2012) (cit. on pp. 1, 6).

[2] P. Fulda, "Evaluation and down selection of corner optical layouts for CE interferometers", CE-T2400012 (2024) (cit. on pp. 1, 7).

[3] K. Izumi and D. Sigg, "Frequency response of the aLIGO interferometer: part 1", LIGO-T1500325 (2015) (cit. on p. 1).

[4] K. Izumi, D. Sigg, and K. Kawabe, "Frequency response of the aLIGO interferometer: part 2", LIGO-T1500461 (2015) (cit. on p. 1).

[5] K. Izumi, D. Sigg, and K. Kawabe, "Frequency response of the aLIGO interferometer: part 3", LIGO-T1500559 (2015) (cit. on p. 1).

[6] K. Kuns, "Impact of cavity lengths and finesse on optical design", CE-G2300048 (2023) (cit. on p. 7).

[7] C. Cahillane, G. L. Mansell, and D. Sigg, "Laser frequency noise in next generation gravitational-wave detectors", Optics Express **29**, 42144 (2021) (cit. on p. 8).

[8] C. Compton, D. Brown, H.-T. Cao, and G. Vajente, "Design requirements document for CHETA: Central HEater for Transient Attenuation", LIGO-T2300387 (2023) (cit. on p. 8).